energies

MDPI

Article

Hydrogen Storage on Porous Carbon Adsorbents: Rediscovery by Nature-Derived Algorithms in Random Forest Machine Learning Model

Hung Vo Thanh [1,2], Sajad Ebrahimnia Taremsari [3], Benyamin Ranjbar [4], Hossein Mashhadimoslem [5,6], Ehsan Rahimi [7], Mohammad Rahimi [8] and Ali Elkamel [6,9,*]

1 Laboratory for Computational Mechanics, Institute for Computational Science and Artificial Intelligence, Van Lang University, Ho Chi Minh City 700000, Vietnam; hung.vothanh@vlu.edu.vn
2 Faculty of Mechanical–Electrical and Computer Engineering, School of Technology, Van Lang University, Ho Chi Minh City 700000, Vietnam
3 Department of Mechanical Engineering, Payame Noor University (PNU), Tehran 19395-4697, Iran
4 Energy Department, Politecnico di Torino, 10129 Torino, Italy
5 Faculty of Chemical Engineering, Iran University of Science & Technology (IUST), Tehran 16846, Iran
6 Department of Chemical Engineering, University of Waterloo, Waterloo, ON N2L 3G1, Canada
7 Department of Materials Science and Engineering, Delft University of Technology, 2628 CD Delft, The Netherlands
8 Department of Biosystems Engineering, Faculty of Agriculture, Ferdowsi University of Mashhad, Mashhad 9177948974, Iran
9 Department of Chemical Engineering, Khalifa University, Abu Dhabi P.O. Box 59911, United Arab Emirates
* Correspondence: aelkamel@uwaterloo.ca

Abstract: Porous carbons as solid adsorbent materials possess effective porosity characteristics that are the most important factors for gas storage. The chemical activating routes facilitate hydrogen storage by adsorbing on the high surface area and microporous features of porous carbon-based adsorbents. The present research proposed to predict H_2 storage using four nature-inspired algorithms applied in the random forest (RF) model. Various carbon-based adsorbents, chemical activating agents, ratios, micro-structural features, and operational parameters as input variables are applied in the ML model to predict H_2 uptake (wt%). Particle swarm and gray wolf optimizations (PSO and GWO) in the RF model display accuracy in the train and test phases, with an R^2 of ~0.98 and 0.91, respectively. Sensitivity analysis demonstrated the ranks for temperature, total pore volume, specific surface area, and micropore volume in first to fourth, with relevancy scores of 1 and 0.48. The feasibility of algorithms in training sizes 80 to 60% evaluated that RMSE and MAE achieved 0.6 to 1, and 0.38 to 0.52. This study contributes to the development of sustainable energy sources by providing a predictive model and insights into the design of porous carbon adsorbents for hydrogen storage. The use of nature-inspired algorithms in the model development process is also a novel approach that could be applied to other areas of materials science and engineering.

Keywords: hydrogen storage; machine learning; random forest; nature-based algorithms

Citation: Thanh, H.V.; Ebrahimnia Taremsari, S.; Ranjbar, B.; Mashhadimoslem, H.; Rahimi, E.; Rahimi, M.; Elkamel, A. Hydrogen Storage on Porous Carbon Adsorbents: Rediscovery by Nature-Derived Algorithms in Random Forest Machine Learning Model. *Energies* **2023**, *16*, 2348. https://doi.org/10.3390/en16052348

Academic Editor: Surender Reddy Salkuti

Received: 31 January 2023
Revised: 22 February 2023
Accepted: 26 February 2023
Published: 28 February 2023

1. Introduction

The demand for ecologically friendly fuels and transportation has grown due to increasing environmental issues [1]. The transition to a hydrogen economy offers one remedy for this purpose [2]. Fuel-cell electric automobiles can use hydrogen as a zero-emission carrier since it has highly desirable characteristics that prevent it from generating carbon dioxide (CO_2) [3,4]. The physical adsorption of hydrogen on solid adsorbents accomplished by extremely large surface areas is one key performance that has received less consideration. Strong reversibility and fast kinetics are two key factors that make this approach beneficial [5]. At the same pressure and temperature, an adsorption process could

provide more hydrogen capability than compression alone. It would also increase safety and provide more design flexibility for the storage tank by enabling the utilization of lower pressures or smaller volumes to hold the same quantity of hydrogen.

Hydrogen can be stored in different adsorbent materials such as nanocomposite and carbon materials. Carbon is one of the best materials for the physical adsorption of hydrogen. The thermal treatment of an appropriate precursor in an inert environment coupled with activation is a typical technique to produce porous carbon compounds with such a large surface area. The process of activation involves the engraving of carbon materials to create pores [6–8]. High surface areas and hierarchical pore structures make supreme micro-and mesopore (<2 nm and 2–50 nm) surface and volume characteristics that facilitate hydrogen adsorption. Microstructures (<2 nm) comparatively play a vital role compared with meso- and macrostructures (2–50 nm and >50 nm, respectively) in porous carbon [9]. It can be performed either "chemically" or "physically" at temperatures ranging from 250 to 600 °C. Physical activation occurs at temperatures between 600 and 1200 °C [10–14]. Recently, innovative porous carbon-based materials, including carbon xerogels, have also been researched [15,16]. Research studies use a method of selecting a carbon precursor, carbonizing and activating it under a variety of treatment parameters, evaluating the hydrogen adsorption, and comparing the findings at a chosen pressure to improve the porous carbon materials to obtain greater hydrogen adsorption values [17–19].

Although there is a consensus in the scientific literature on the value of intersecting fields in micropores for enhancing excess hydrogen absorption, the intensity or the nature of this relationship has not been able to be quantified. Various parameters influence the porous carbon adsorption performance. The porous carbon can be mostly obtained by chemical activating processes that are employed by chemical activating alternatives such as KOH, ZnCl, acetone, etc. [13,20]. Hence, demonstrating the relations between the chemical activation and the distribution of pore sizes and hydrogen uptake is complex. While some researchers suggest the reverse, Sethia and Govind showed that optimized porosity is more significant than having a wide surface area [21]. Only by quantitatively determining the relative relevance of the pertinent factors could such inconsistencies be addressed. In other instances, it is even impossible to determine whether a given factor aids or has no impact on absorption. The question of how oxygen concentration influences adsorption is one instance that can be discovered in both theoretical and experimental research. By applying both approaches, the idea that oxygen concentration enhances sorption can be confirmed [22]. In addition, there is research that disputes this idea [23]. This research's inconsistent findings make it impossible to optimize carbon materials via logical design, since it is unclear as to which aspects are crucial and how much they contribute. Often, computational research involving quantum chemistry or molecular simulation has the potential to tackle problems of this nature. However, the majority of theoretical studies in the field typically focus on only studying specific types of carbon nanomaterials [24,25], leaving it unclear as to whether they can be oversimplified to other, particularly amorphous, forms of carbon.

Artificial intelligence or machine learning (ML) approaches have an ascending trend in parallel, assisted, and post-evaluation experimental results. ML approaches have been developed in multidisciplinary subjects [26,27]. This is because it is challenging to design models that are representative of actual porous carbon materials. This provides a critical information gap that is unlikely to be filled using experimental methods. A crucial challenge lies in determining whether the knowledge gained from conceptual or experimental research could be utilized to later forecast the characteristics of those other materials having comparable structural and chemical features in a consistent, effective, and informative way. This is the target of the ML technique, which uses patterns in data to be automatically identified [28–30]. ML frequently employs methods from data analysis. While ML creates frameworks that could be used to generate forecasts, data analysis enhances the exact solutions. As a result, ML could indeed determine connections between

the chemical and structural formations of porous materials, as well as their abilities for the adsorption process, from the data. These connections could then be used to forecast the adsorption characteristics of the novel's as-yet unsynthesized components [31–33]. Table 1 illustrates the ML-based research on hydrogen storage with multiple objectives and ML models.

Table 1. The previous works of literature on hydrogen storage via machine learning.

Modeling Process	ML Model	R^2	Ref.
The filling tank modeling based on the conditional features	ANN	0.99	[34]
Modeling, considering structural and conditional parameters	ANN	-	[35]
Micro-textural and porosity features at fixed condition parameters)	SVM	0.98	[33]
Structural and conditional parameters utilized	ANN	0.95	[36]
Novel nature-derived algorithms predict the performance of porous carbon for hydrogen storage.	RF_ (GA, DA, GWO, and PSO)	0.98	This work

ANN = Artificial neural network, SVM = Support vector machine, RF = Random Forest, GA = Genetic algorithm, DA = Dragonfly algorithm, GWO = Grey wolf optimization, and PSO = Particle swarm optimization.

The intricate nonlinear interactions between many parameters have been studied using ML algorithms utilizing a wide range of research data on hydrogen adsorption in carbon-based materials [37–39]. In a simple ML model, Yangzesheng et al. presented a meta-learning technique to predict H_2 adsorption as a factor of both pressure and temperature for various nanoporous materials. They created the model, utilizing an encoder–decoder structure to identify hydrogen adsorption fingerprints for nanoporous materials in their original forms [40].

As mentioned before, conventional algorithms such as artificial neural networks (ANNs) are effectively applied in gas adsorption prediction. Nature-derived algorithms are regarded as novel ML techniques that effectively perform predictive performance. As shown in Figure 1, this type of algorithm is powered by natural inherent patterns such as animal groups, the universe, and the living world. In this study, four nature-based algorithms were applied to predict hydrogen uptake values on porous carbon materials of biochar, activated carbon (AC), and metal-doped carbon. Multi-features such as adsorbent types, chemical activating agents (KOH, ZnCl, etc.), micro-structural, and conditional features are used as input variables. Nature-inspired algorithms possess higher feasibility and accuracy with qualitative inputs, and facilitate the computational costs. The objectives of this purpose can be stated in the following points:

- Hydrogen storage on porous carbon materials is achieved through a rediscovery data-driven approach using the random forest ML model.
- Considering the chemical activating agents and adsorbent types as inputs for the model.
- The evaluation of the accuracy of the prediction of nature-derived algorithms for hydrogen storage.
- Feasibility of grey wolf optimization (GWO), dragonfly algorithm (DA), particle swarm optimization (PSO), and genetic algorithm (GA) in various ranges of data sizes.

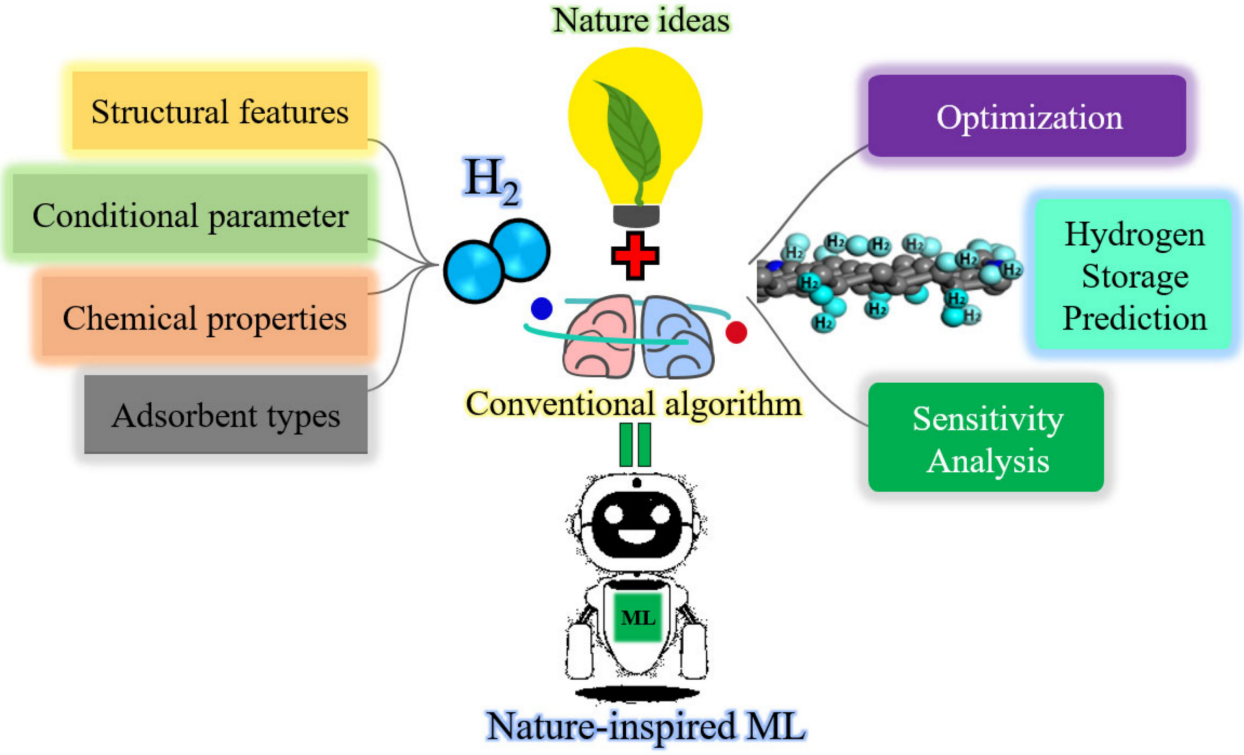

Figure 1. Nature-inspired algorithms in ML for hydrogen storage prediction.

2. Material and Methods

2.1. Sample Data Collection

The works of literature related to hydrogen storage using porous carbon were evaluated to collect the information for the dataset preparation. The extracted data, 566 datasets from previous scientific reports, were applied to construct and test smart ML models. The information preparation process was applied by using keywords such as: "metal-doped", "activated carbon", and "porous carbon", with the combination of "hydrogen storage", and "H_2 uptake". Biochar, activated carbon, and metal-doped carbon as adsorbent materials were detected. The related structural, activating, and conditional parameters were extracted for the modeling process. Figure 2 shows the dataset provision and modeling implementation procedures. The details of calculating the variables and raw datasets are provided in the Supplementary Materials Section (SI).

Eleven independent variables are considered for constructing the RF model to predict hydrogen storage capacity, as shown in Table 2. They are divided into four categories including solid adsorbent, chemical activating, structural characteristics, and conditional parameters. The first category consists of porous carbon types such as biochar, activated carbon, and metal-doped carbon. The second includes chemical activating agents and ratios. The chemical agents mostly possess alkali, acidic, and metal chloride types. The textural features are specific surface area, micro-/mesopore volume, total pore volume, and average pore diameter. Finally, the conditions consist of temperature and pressure features. The ratio of activating agents is calculated using the following equation:

$$AR = \frac{m_A}{m_C} \quad (1)$$

where m_A and m_C are the mass of the activation agent and the mass of the carbon precursor, respectively.

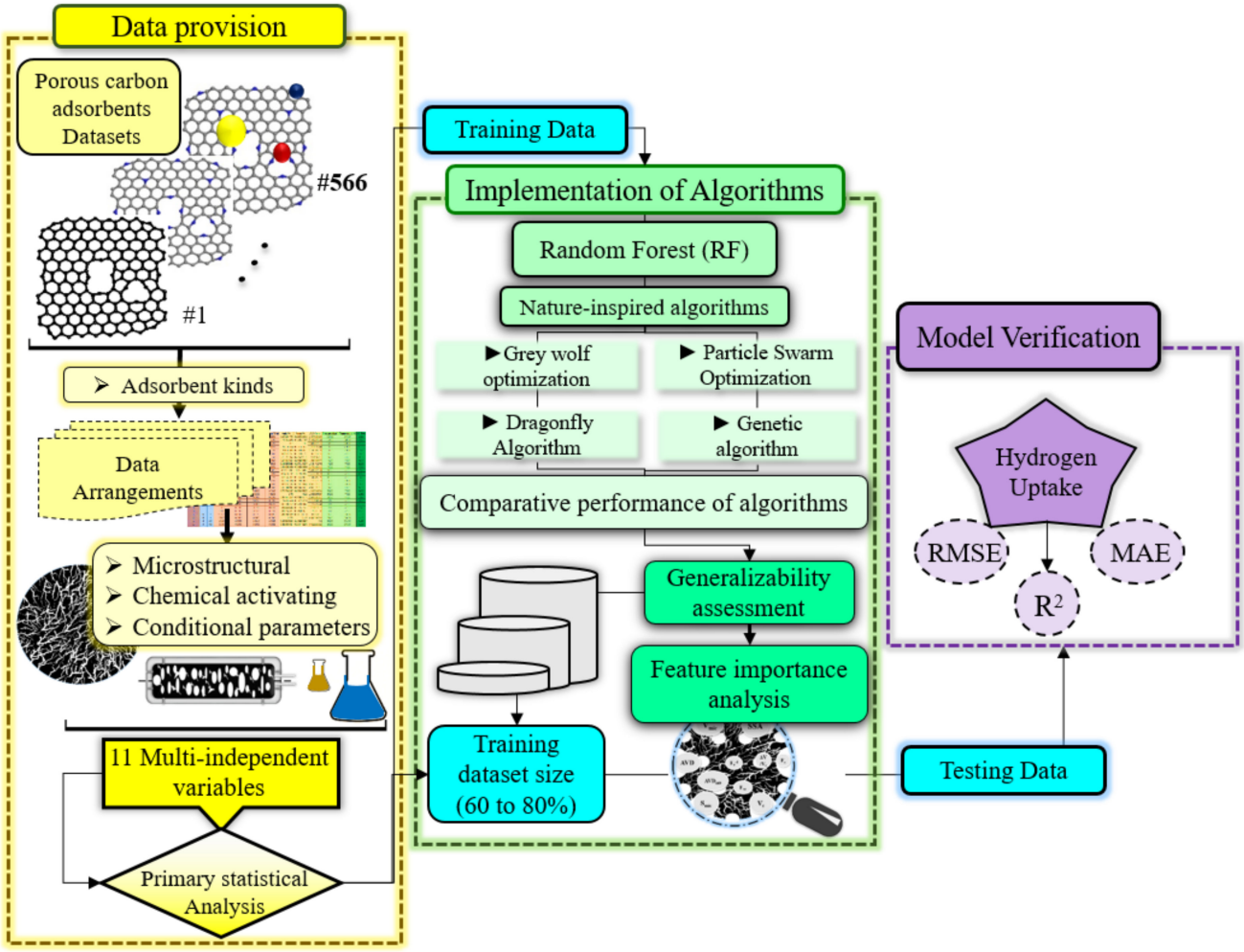

Figure 2. The process of datasets preparation and modeling via ML.

Table 2. The description of independent variables and output.

Category	Input	Symbol	Unit
Solid adsorbents	Adsorbent kind $_{NQ}$	AK	-
Chemical activating	Activating Agent $_{NQ}$	AA	-
	Activating Ratio	AR	-
Structural features	Specific surface area	SSA	m^2g^{-1}
	Micropore volume	V_{mic}	cm^3g^{-1}
	Mesopore volume	V_{mes}	cm^3g^{-1}
	Total pore volume	Vt	cm^3g^{-1}
	V_{mic}/V_t	Fv	-
	Average pore diameter	AVD	nm
Conditional parameters	Pressure	P	bar
	Temperature	T	K
Storage	Hydrogen	H_2	%wt

2.2. The Smart Machine-Learning Model

Random forests (RFs) are a set of approaches consisting of the construction of decision tree collecting, derived from a randomly varying tree orientation program. The decision trees are prominent options to address the related challenges as they exhibit low bias and large variation. These make them very probable to benefit from an optimization model [41].

Figure 3 displays the random forest approach for the regression issue. The procedure of the RF model for training data is summarized as follows [42]: (i) Select generated data points randomly from the training sample. (ii) Construct a tree structure connected with the number of data samples. (iii) Select the number N of trees for a certain aim to develop and repeat steps 1 and 2. (iv) For new data samples, forecast the value for the data sample using each of the N-tree trees, and exhibit the new data sample to the average of all anticipated values. Indeed, this ML model provides a deep understanding of the decision tree by controlling the level of nonlinearity in the training database [41,43]. Each tree is generated based on the randomly selected subset of the variables in the decision tree-building process, and creates various results from different trees. The average marks of all the decision trees are determined as the outcomes of the RF models [44]. This objective is completed by switching Out-of-Bag (OOB) samples from a specific predictor to estimate the increase in evaluation error, while the remaining parameter is kept the same. The mean square error (MSE_{OOB}) is determined as follows [41,45]:

$$MSE_{OOB} = \frac{1}{N_T} \sum_{i=1}^{N_{DT}} \left(h_i - \hat{h}_i \right)^2 \quad (2)$$

where N_{DT} stands for the number of OOB samples, and $\hat{h}_i$ represents the OOB prediction for training data samples. The Sciki-learn toolkit, namely "sklearn.ensemble.RandomForest-Regressor", was used to train and test the RF models [46]. The tuning hyperparameter was optimized by nature-inspired algorithms that are introduced in the next section.

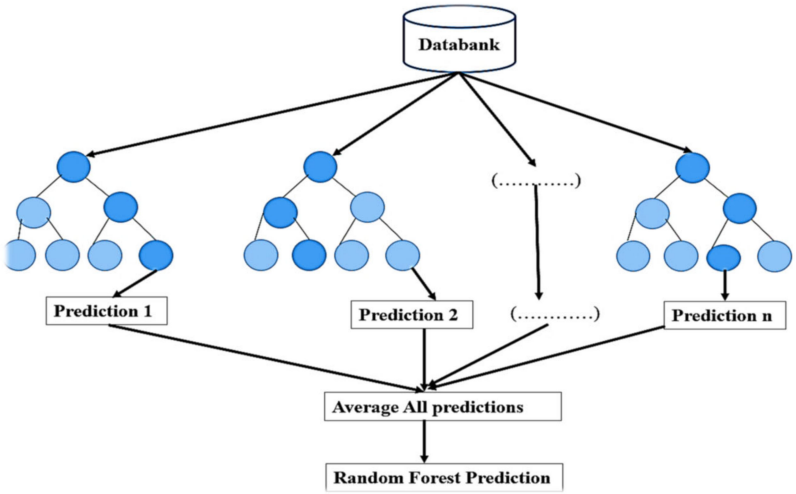

Figure 3. The schematic of the random forest technique for a regression problem. Solid color means that the prediction is correct, while the light color means that the prediction is incorrect.

Thus, before the RF model in the training process, the data must be normalized over the range of [0, 1]. The popularly applied method of normalization and of processing the data linearly over a constant range is as follows:

$$x_n = \left(\frac{x - x_{min}}{x_{max} - x_{min}} \right) \times (r_{max} - r_{min}) + r_{min} \quad (3)$$

where x, x_n show the original data and all the normalized variable values. In addition, $x_{\min,max}$ correspond to the maximum and minimum values of the variable, respectively. $r_{\text{maxand } min}$ present the desired values of the transformed variable range. The hydrogen uptake dataset is randomly shuffled and repeated to obtain the properly placed segmentation. In total, 60 to 80% of all porous carbon samples were randomly selected for the training phase, and 40 to 20% of them were chosen.

2.3. Nature-Inspired Methods

2.3.1. Particle Swarm Optimization (PSO)

Among the most popular optimization routes utilized in technology is particle swarm optimization, or PSO for short. This is because of its effectiveness, ease of use, and general application. In 1995, Eberhart and Kennedy presented one of the most well-known randomized algorithms as a strong optimal control tool [47]. Like a flock of birds or a swarm of fish, it moves in a group. Well-researched coverage of the idea, modifications, and significant applications in power grids could be found in [48]. To optimize the tuning hyperparameters by tuning the RF model, the following steps were considered: (1) Making a swarm of particles with random beginning positions and velocities. (2) Objective function computation for tuning parameters. (3) Upgrading each particle's position and velocity based on an analysis of its optimal location relative to that of the total population. (4) These procedures are repeated up to some maximum number of times, or until some halting requirement is achieved.

2.3.2. Genetic Algorithm (GA)

The genetic algorithm (GA) is an important tool related to genetic populations, to determine the optimal functions [49,50]. GA stands for one branch of evolutionary calculation that includes the following steps: genetics, mutation, natural selection, and crossover [51]. A set of preliminary candidates is produced, and their respective computed values are determined [52]. The processing of GA could be highlighted as follows: (i) Population origination: This stage randomly creates a population of n individuals. (ii) Determine the adaptive values: The phase evaluates the adaptation of each individual. (iii) Selection: The process chooses two members of the population, depending on their adaptability. (iv) Crossover: A crossover between two parents is created to generate a new individual. (v) Mutation: For each possible variant picked, new individuals are produced. (vi) Select the result: The GA algorithm finishes while the stopping constraint is achieved, and the optimal solution is provided for the present population. If the stopping conditions are not fulfilled, the new group will be perpetually formed by repeating the three steps (selection, crossover, and mutation). Several subsurface ML-based studies have used the grid search for tuning the ML models [53]. However, GA might be better in terms of the optimization problems. Thus, this study used GA to propose hybrid ML models by coupling GA-RF for better regression prediction.

2.3.3. Grey Wolf Optimization (GWO)

The majority of grey wolves are group animals. On the whole, one should expect to be in a group of between 5 and 12 individuals. Among them, the norms of social dominance are quite rigid. The following steps are the key processes of a grey pack of wolves, according to [54]:

- The alpha wolves are the ones who dominate the pack and who make all the important calls. The pack must follow the alpha's lead at all times.
- They are the alpha's subordinates, and they aid the alpha in deciding and in carrying out various tasks. The beta is the most likely choice for alpha.
- The alpha is the scapegoat. The alpha wolf must always take a back seat to the pack's other alphas. Only these wolves are given food anymore.
- Deltas are submissive to alphas and betas, but they hold the upper hand over omegas. This group includes watchmen, guardians, elders, hunters, and caretakers. Scouts keep an eye on the territory's fringes and sound the alarm if they see any trouble. The oldest wolves are the seasoned former pack leaders. Hunters aid the pack's alphas and betas in their pursuit of prey and in supplying the pack with food.

The optimal solution in the GWO computer formula is denoted by the letter "alpha." Beta and delta are the names of the second- and third-best options. We will assume that omega is the case for the remaining potential answers.

2.3.4. Dragonfly Algorithm (DA)

In comparison to other optimization algorithms, the Dragonfly algorithm (DA) is a relatively new metaheuristic algorithm. It performs well when faced with a variety of optimization problems such as continuous, single-objective, and multi-objective optimization [55]. Dragonflies operate in small groups in search of food in nature; this process is called hunting mechanisms. Larger groups of dragonflies fly together in one direction, causing the swarm to migrate in a process known as the migration mechanism [56]. Five processes define the swarming behaviors of dragonflies [57]:

(a) Distancing one from the others to reduce the risk of a static accident is known as "separation".
(b) The term "alignment" describes how one search agent's speed corresponds to the speeds of similar agents in the area.
(c) The terms "attraction" and "distraction" refer to the allure of the food supply for migrating creatures, and the human impulse to flee from danger, respectively.

2.4. Optimization of Tuning Parameters

The random forest model and four nature-inspired algorithms have tuning parameters that need to be optimized. As shown in Table 3, four statistical parameters are optimized. These features are evaluated in range and optimal value. The ideal value of estimators is determined as 175, and the max depth is set as 21. The tuning parameters of the algorithms are optimized, as shown in Table 4. The variables of nature-derived algorithms are optimized, and the values are determined. For example, the tuning variables of GA for population size, mutation rate, the number of iterations, and the selective pressure, are 25, 0.05, 25, and 2. Two main variables of PSO include the size of the swarm and the number of iterations, which are 100 and 25. Other algorithms are optimized with the same process that is applied in the ML model.

Table 3. The optimal tuning parameters of RF were optimized by considering nature-inspired methods.

Method	Tuning Parameter	Range	Optimal Value
Random Forest (RF)	Number of estimators	10–1000	175
	Max features	0–20	0.263
	Min samples leaf	1–40	1
	Max depth	5–500	21

Table 4. The parameter setting is considered for each optimization method.

Method	Variable	Values
Dragonfly algorithm (DA)	Population size	50
	Timeout	60×60
	Number of iterations	25
Grey wolf optimization (GWO)	Number of wolves	80
	Number of iterations	25
	a	Linearly decreased from 4 to 0
Particle swarm optimization (PSO)	Size of swarm	100
	Number of iterations	25
	c_1	2.05
	c_2	2.05
	γ	0.659
Genetic algorithm (GA)	Selective pressure	2
	Population size	25
	Mutation rate	0.05
	Number of iterations	25

2.5. Evaluation Criteria

The Pearson correlation coefficient (PCC) was utilized to measure the linear dependence between all dependent and independent variables. The PCC was conducted to check the collinearity value and the linear correlation between the independent and dependent variables. The existence of linear dependence between the variables is determined as follows:

$$\mathrm{PCC} = \frac{\sum_{i=1}^{n}(x_i - \overline{x})\sum_{i=1}^{n}(y_i - \overline{y})}{\sqrt{\sum_{i=1}^{n}(x_i - \overline{x})^2}\sqrt{\sum_{i=1}^{n}(y_i - \overline{y})^2}} \tag{4}$$

where x and y represent the independent and dependent variables, and $\bar{x}$ and $\bar{y}$ are their mean values. The significant levels based on the correlation coefficient are calculated as:

$$t = \frac{PCC\sqrt{N-2}}{\sqrt{1-PCC^2}} \tag{5}$$

where N represents the number of samples.

Three criteria were appraised to evaluate the performance of the machine learning (ML) technique. These abovementioned criteria are presented in the previous studies used to predict the reliability of the output accuracy. Root mean square error (*RMSE*), mean absolute error (*MAE*), and the coefficient of determination (R^2) can evaluate the accuracy of models as follows:

$$MAE = \left(\sum_{r=1}^{N}\frac{|H_r - H_p|}{N}\right) \tag{6}$$

$$RMSE = \sqrt{\left(\sum_{r=1}^{N}|H_r - \hat{H}_p|^2\right)/(N-1)} \tag{7}$$

$$R^2 = 1 - \sum_{1}^{N}(H_r - H_p)^2 / \sum_{1}^{N}(H_r - \hat{H}_r)^2 \tag{8}$$

where H_r and H_p indicate the real and predicted values, and $\hat{H}_p$ is the average of the predicted values.

3. Results and Discussion

3.1. Initial Correlation Evaluation

The initial statistical criteria are provided in Table 5. The specific surface area is approximately between 0 and 4300 m^2g^{-1}. The range of pore volume is 0 to 2.6 cm^3g^{-1}. The conditional features such as temperature and pressure are mostly 77 to 303, and 1 to 270 bar, respectively.

Table 5. The statistical criteria of input features for hydrogen storage in porous carbon.

Quantitative Feature	Minimum	Average	Maximum	Stedv
Ratio	0	2.24	5	1.5798
SSA (m^2g^{-1})	0.42	2207.438	4310	1009.4183
V_{mic} (cm^3g^{-1})	0	0.84	2.01	0.5098
V_{mes} (cm^3g^{-1})	0	0.33	1.8	0.3625
V_t (cm^3g^{-1})	0	1.17	2.6	0.5973
V_{mic}/V_t	0.03	0.72	1	0.2255
AVD (nm)	0.24	2.01	4.43	0.5177
Pressure (bar)	1	35.55	270	43.3089
Temperature (K)	77	142.93	303	98.7025
H_2 (%wt)	0	2.811	12.6	2.3539

Principally, the Pearson correlation coefficient (PCC) matrix is used to disclose the variables' relations to each other. Figure 4 illustrates all input variables compared with hydrogen uptake, which distinguishes the significant level and the correlation coefficient. Hydrogen uptake was notably exhibited a highly significant level with chemical activating, micro-structural, and operational variables ($p < 0.01$). The p-value indicates the reliability of the linear relationship of correlation, where all variables prominently have high p-value levels. Nevertheless, the correlation between H_2 storage and AVD was not significant. The activating agent ratio (AR), activating agent type (AA), and adsorbent kind (AK) were correlated with H_2 uptake 0.392, 0.291, and 0.271, with p-value < 0.01, respectively. Adsorbent kinds consist of bio-char, activated carbon, and metal doped-AC. ACs and metal-doped ACs such as Ni-AC, Pb-AC, etc., significantly can adsorb hydrogen, with as high a porosity as compared with biochar [58]. ACs exclusively perform the hydrogen uptake by physisorption in cryogenic temperatures at a specific surface area of ~4000 m^2g^{-1} [22,59]. Metal-doped ACs donate the active sites on the carbon surface for storage, even with low porosities [60,61]. Furthermore, the chemical activating processes donate high porosities to the carbon structure, which facilitates the hydrogen storage on the porous carbon. Alkali agents are the most popular with post-purifying using diluted acid (HCl) [62,63]. Thus, the correlation coefficient between the independent variables was observed. AA and AR are correlated with SSA and V_{mic}, at 0.286 to 0.485 with p-value < 0.001. The specific surface area (SSA) and total pore volume (V_t) have a significant level p-value < 0.001 and a high correlation of 0.438 and 0.293 for hydrogen uptake. This is because the hydrogen uptake is facilitated by low-temperature conditions (77 K). Hence, the correlation value between the H_2 storage and temperature is −0.605.

AK	0.489 (0.000)	0.577 (0.000)	0.119 (0.005)	-0.193 (0.000)	0.138 (0.001)	-0.086 (0.041)	-0.13 (0.002)	-0.095 (0.024)	-0.07 (0.097)	-0.214 (0.000)	0.271 (0.000)
AA		0.555 (0.000)	0.485 (0.000)	0.286 (0.000)	0.163 (0.000)	0.341 (0.000)	0.024 (ns)	-0.03 (ns)	0.016 (ns)	-0.087 (0.038)	0.291 (0.000)
AR			0.322 (0.000)	-0.003 (ns)	0.218 (0.000)	0.132 (0.002)	-0.125 (0.003)	-0.088 (0.037)	-0.045 (ns)	-0.270 (0.000)	0.392 (0.000)
SSA				0.736 (0.000)	0.397 (0.000)	0.883 (0.000)	-0.083 (0.050)	0.21 (0.000)	-0.003 (ns)	-0.036 (ns)	0.438 (0.000)
V_{mic}					-0.117 (0.005)	0.782 (0.000)	0.369 (0.000)	0.299 (0.000)	0.025 (ns)	0.144 (0.001)	0.204 (0.000)
V_{mes}						0.499 (0.000)	-0.818 (0.000)	0.326 (0.000)	-0.055 (0.190)	-0.139 (0.001)	0.186 (0.000)
V_t							-0.174 (0.000)	0.47 (0.000)	-0.031 (ns)	0.042 (ns)	0.293 (0.000)
F_v								-0.265 (0.000)	0.022 (ns)	0.128 (0.002)	-0.162 (0.000)
AVD									-0.03 (ns)	0.116 (0.006)	-0.068 (ns)
P										0.471 (0.000)	-0.114 (0.007)
T											-0.605 (0.000)
H_2											

Figure 4. Pearson correlation matrix of the input variables and hydrogen uptake as an output variable. The values display the value of the correlation and the significance levels in parentheses between all variables.

Finally, it can be noted that AR, AA, and AK of the chemical activating process is positively correlated with hydrogen storage. Following it, the structural characteristics such as surface and porosity in the range of 2–50 nm are highly appropriate to be considered as input for the Ml model. The cryogenic storage of hydrogen at 77 K is significantly correlated with H_2 uptake, with a *p*-value < 0.001. As temperature possesses a high importance, the pressure comparatively showed a low correlation coefficient.

3.2. H_2 Uptake Prediction

The random forest (RF) ML model is selected as the base of the modeling process for hydrogen uptake prediction. As shown in Figure 5, four algorithms were effectively merged with RF that showed a superior ability for hydrogen storage prediction. R^2 approximately achieved ~0.98 for the training phase. Although the test accuracy descended which it obtained 0.91 to 0.93, the results were still satisfying enough. Particle swarm and gray wolf optimizations (PSO and GWO) in the RF model exhibited the same results in the train and test phases as R^2 of ~0.98 and 0.91, respectively. The genetic algorithm (GA) leads a bit higher in hydrogen prediction in the test phase (R^2 of ~0.93). In addition, the RF_Dragonfly algorithm (RF_DA) indicated a precise prediction performance of 0.98 and 0.90 in the train and test steps, respectively. The differences in population size are tuned based on the algorithm's optimization and computational resources. In addition, the train dataset sizes are randomly evaluated as 60 to 80% from 566 datasets, and the best accuracies are achieved at 80% and 20% in the train and test phases, respectively.

3.3. Generalizability Evaluation

The feasibility of algorithms to predict the hydrogen uptake value can be compared using generalizability analysis. As illustrated in Table 6, the R^2 criteria of algorithms, specifically the grey wolf algorithm, exhibited a high accuracy in the training phase, at 0.99 of R^2. The accuracy in the train size (TS) of 60% to 80% approximately achieved ~0.84 to 0.92 of R^2 in the test phase, respectively. These results are repeated for other algorithms: dragonfly, genetic, and particle swarm optimization algorithms. By decreasing the training size from 80 to 60%, RMSE and MAE are 0.6 to 1, and 0.38 to 0.52.

Table 6. The three criteria of RMSE, MAE, and R^2 in various training dataset sizes (TS).

Training Size (TS)	Algorithm	*RMSE*		*MAE*		R^2	
		Train	**Test**	**Train**	**Test**	**Train**	**Test**
60%	RF_PSO	0.339	0.994	0.184	0.505	0.980	0.836
	RF_GA	0.337	0.964	0.185	0.524	0.981	0.848
	RF_DA	0.336	0.990	0.186	0.500	0.9805	0.836
	RF_GWO	0.335	0.978	0.185	0.496	0.979	0.834
70%	RF_PSO	0.296	0.623	0.181	0.387	0.9862	0.9216
	RF_GA	0.290	0.641	0.184	0.420	0.9867	0.9241
	RF_DA	0.293	0.664	0.186	0.420	0.9865	0.9183
	RF_GWO	0.286	0.631	0.183	0.409	0.9870	0.9263
80%	RF_PSO	0.313	0.667	0.184	0.420	0.9848	0.9106
	RF_GA	0.284	0.598	0.175	0.387	0.9873	0.9281
	RF_DA	0.297	0.649	0.181	0.400	0.9863	0.9168
	RF_GWO	0.291	0.624	0.179	0.377	0.9865	0.9215

3.4. Sensitivity Analysis

Sensitivity analysis is achieved based on the measured relevancy score to investigate the impact of the inputs on hydrogen storage. As can be seen in Figure 6, temperature and pressure contain the 1 and 0.3 scores in the first and sixth ranks. In addition, the micro-structural variables of total pore volume, SSA, and V_{mic} exhibit scores of 0.48 in the second to fourth ranks. The average pore diameter and mesopore volume have 0.28

and 0.24 scores. These values comparatively are low in comparison with the other values. Adsorbent kinds (biochar, activated carbon, and metal-doped carbon) comparatively have a score of 0.18.

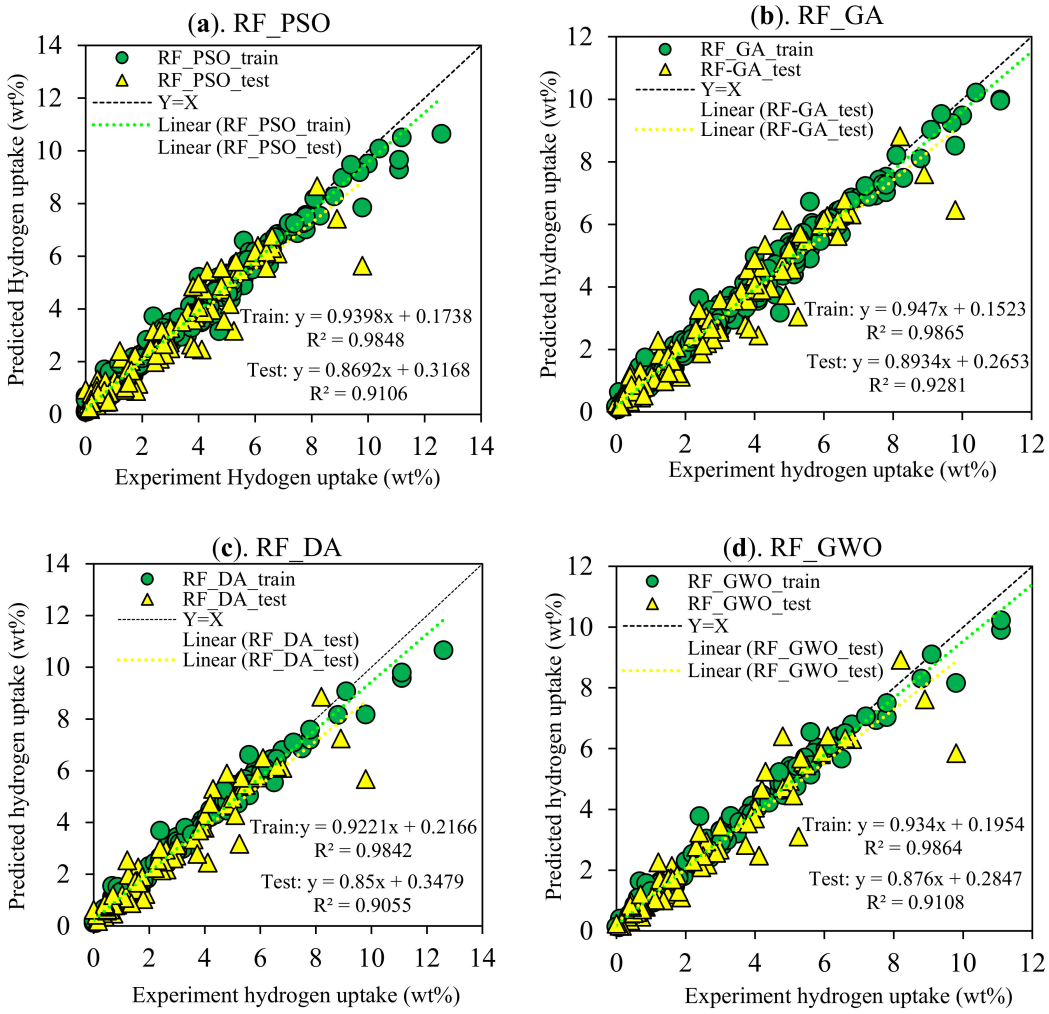

Figure 5. Observing the real and predicted values of hydrogen uptake on porous carbon in the train and test phases (circles and triangles represent the real and predicted values, respectively).

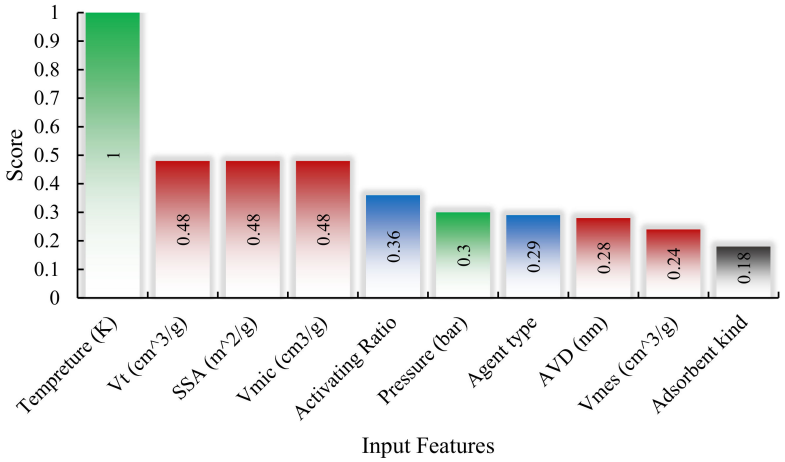

Figure 6. The relevancy score illustrates the impact of the independent variables on hydrogen storage. The green color means conditional parameters, red color means structure of characteristics, blue means chemical activation parameter, and the grey color means type of adsorbents.

4. Conclusions and Further Research

In this study, hydrogen uptake is modeled using four nature-inspired algorithms in the random forests (RFs) model. Four main categories include the characteristics of adsorbent type, chemical activation, and the micro-structural and operational conditions modeled using the RF model. The ML assessment accurately predicted the porous carbon adsorbents for hydrogen storage. Dragonfly, grey wolf, particle swarm, and genetic optimization algorithms exhibited 0.91 to 0.93 and 0.99 of R^2 for the test and train phases, respectively. Moreover, the generalizability analysis in the training size area of 60 to 80% leads to accuracies of 0.29 to 0.34 of RMSE, 0.18 to 0.19 of MAE, and 0.99 of R^2 in the training phase. In the test phase, these values achieved 0.6 to 1, 0.4 to 0.5, and 0.84 to 0.93, respectively. The sensitivity analysis demonstrated the ranks for temperature, total pore volume, specific surface area, and micropore volume in first to fourth, with relevancy scores of 1 and 0.48. The RF model as a machine learning (ML) technique endorses the computational approach to achieve the advanced H_2 energy storage objectives. The contribution can be stated in several points such as: (i) This work creates ML models to estimate the hydrogen storage capacities of different porous carbon adsorbents. This model may be used to guide the design of novel adsorbents for hydrogen storage, a crucial step in the development of renewable energy sources. (ii) The nature-inspired algorithms such as GWO, DA, GA, and PSO choose the model's most pertinent characteristics. These algorithms are well-known for discovering optimal solutions to complicated problems, as they are based on evolution and the swarm behavior observed in nature. (iii) The achievements have demonstrated that using nature-inspired methods to pick model features enhances the model's accuracy. In addition to its accuracy and resilience, the random forest algorithm is a useful approach to estimating the hydrogen storage capacities of porous carbon adsorbents. (iv) The survey sheds light on the connection between the structural characteristics of carbon materials and their hydrogen storage capacities. This can inform the creation of novel hydrogen storage materials with optimal architectures.

5. Limitations and Future Works

The porous carbon-based adsorbent materials with various synthesizing processes for hydrogen storage attracted an ascending trend, as shown in Figure 7. Thus, researchers will be faced with a high quantity of experimental works and datasets. On the other hand, the importance of multi-features for porous carbons is observed through machine learning (ML) techniques. This approach is fast and helpful for designing the optimal porous carbon adsorbents. The limitations can be emphasized below:

- Although ML models achieve high predictive performances or optimizations, in-depth independent variables are needed for advanced evaluation. The variables can be introduced as energy bonds, adsorption energy, bond angles, etc.
- To save time, costs, and the reuse of datasets, a platform for archiving datasets should be designed so that ML researchers can access big data.
- The qualitative features such as biomass precursors, inherent constituents, and lignocellulose portions must be simplified for smart modeling.

Future ML studies can propose dialectic algorithms to tune synthesizing variables based on the precursors for adsorbent materials. In addition, upcoming modeling research can be constructed using molecular-based variables for the smart monitoring of the optimal state of gas adsorption, and specifically, hydrogen uptake.

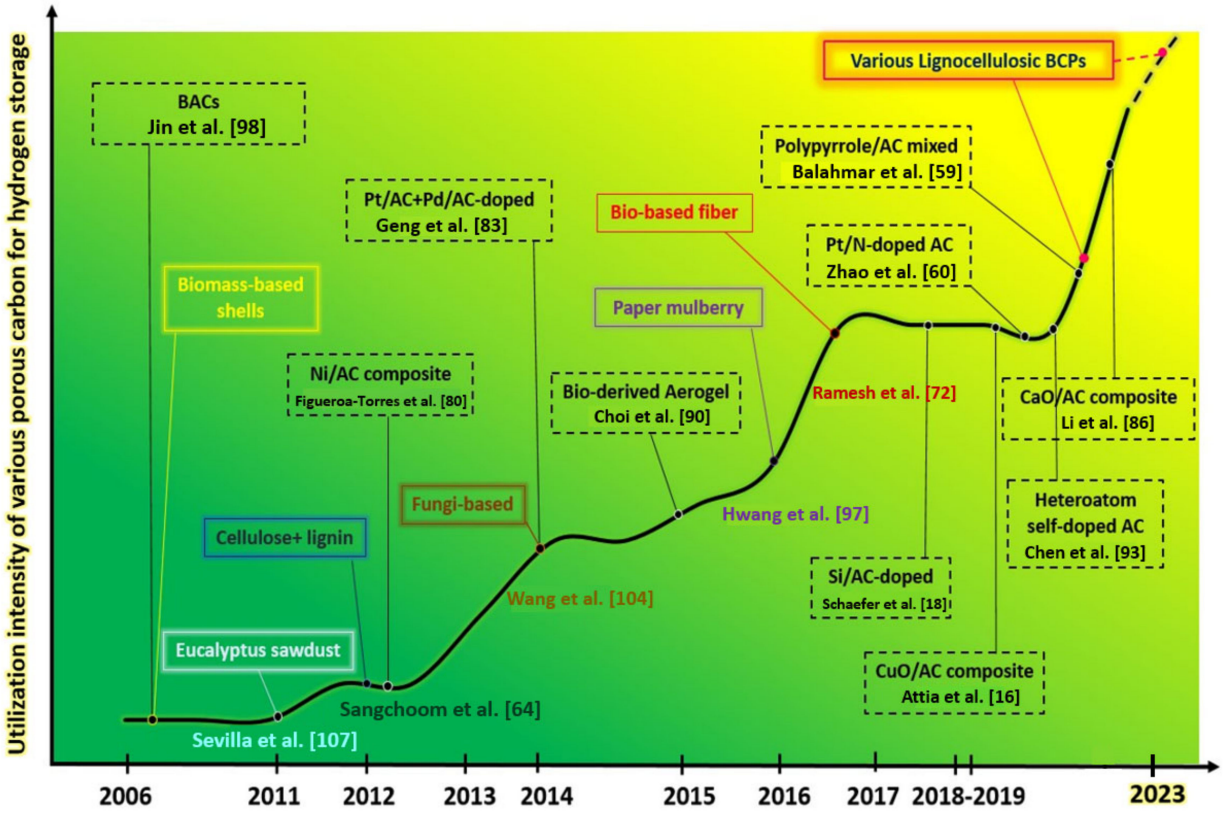

Figure 7. The review of studies utilized various precursors to synthesize various porous adsorbent materials for hydrogen storage [16,18,33,59,60,64,72,80,83,86,90,93,97,98,104,107].

Supplementary Materials: The following supporting information can be downloaded at: https://www.mdpi.com/article/10.3390/en16052348/s1, SI file includes some equations for variables calculations and datasets with corresponding references. Table S1. The datasets extracted from previous experimental studies in hydrogen storage on porous carbons. References [64–109] are cited in the supplementary materials.

Author Contributions: Conceptualization, H.V.T., B.R., H.M., E.R., M.R. and A.E.; Methodology, H.V.T., S.E.T., B.R., H.M., E.R., M.R. and A.E.; Software, H.V.T. and M.R.; Validation, H.V.T. and M.R.; Formal analysis, H.V.T., B.R., S.E.T., H.M., E.R. and M.R.; Data curation, H.V.T.; Writing—original draft, H.V.T., B.R., S.E.T., H.M., E.R. and M.R.; Writing—review & editing, H.V.T., B.R., S.E.T., H.M., E.R. and M.R.; Supervision, A.E.; Project administration, H.V.T., M.R. and H.M.; Funding acquisition, A.E. All authors have read and agreed to the published version of the manuscript.

Funding: This research received no external funding.

Data Availability Statement: Data Availability Statements are available in Supplementary Materials.

Conflicts of Interest: The authors declare no conflict of interest.

Nomenclature

AC	Activated carbon
AK	Adsorbent kind
AVD	Average pore diameter
AA	Activating agent
AR	Activating ratio
BCPs	Biomass-based carbon precursors
BACs	Bio-derived ACs
DA	Dragonfly algorithm

GA	Genetic algorithm
GWO	Grey wolf optimization
ML	Machine learning
OOB	Out-of-Bag
PSO	Particle swarm optimization
R^2	Mean square error
RMSE	Root mean square error
RF	Random forest
SSA	Specific surface area
Vt	Total pore volume
V_{mic}	Micropore volume
V_{mes}	Mesopore volume

References

1. Lu, D.; Hu, D.; Yi, F.; Li, J.; Yang, Q. Optimal Selection Range of FCV Power Battery Capacity Considering the Synergistic Decay of Dual Power Source Lifespan. *Int. J. Hydrogen Energy* **2023**. [CrossRef]
2. Hu, D.; Wang, Y.; Li, J.; Yang, Q.; Wang, J. Investigation of Optimal Operating Temperature for the PEMFC and Its Tracking Control for Energy Saving in Vehicle Applications. *Energy Convers. Manag.* **2021**, *249*, 114842. [CrossRef]
3. Sharma, S.; Ghoshal, S.K. Hydrogen the Future Transportation Fuel: From Production to Applications. *Renew. Sustain. Energy Rev.* **2015**, *43*, 1151–1158. [CrossRef]
4. Ströbel, R.; Garche, J.; Moseley, P.T.; Jörissen, L.; Wolf, G. Hydrogen Storage by Carbon Materials. *J. Power Sources* **2006**, *159*, 781–801. [CrossRef]
5. Barthélémy, H.; Weber, M.; Barbier, F. Hydrogen Storage: Recent Improvements and Industrial Perspectives. *Int. J. Hydrogen Energy* **2017**, *42*, 7254–7262. [CrossRef]
6. Kunowsky, M.; Marco-Lozar, J.P.; Oya, A.; Linares-Solano, A. Hydrogen Storage in CO_2-Activated Amorphous Nanofibers and Their Monoliths. *Carbon N. Y.* **2012**, *50*, 1407–1416. [CrossRef]
7. Lee, S.-Y.; Park, S.-J. Influence of CO2 Activation on Hydrogen Storage Behaviors of Platinum-Loaded Activated Carbon Nanotubes. *J. Solid State Chem.* **2010**, *183*, 2951–2956. [CrossRef]
8. Rahimi, M.; Abbaspour-Fard, M.H.; Rohani, A. A Multi-Data-Driven Procedure towards a Comprehensive Understanding of the Activated Carbon Electrodes Performance (Using for Supercapacitor) Employing ANN Technique. *Renew. Energy* **2021**, *180*, 980–992. [CrossRef]
9. Toda, I.; Komatsu, K.; Watanabe, T.; Toda, H.; Akasaka, H.; Ohshio, S.; Saitoh, H. Effect of Meso- and Micropore Structures on the Hydrogen Storage Properties of Nanoporous Carbon Materials. *J. Porous Mater.* **2018**, *25*, 1765–1770. [CrossRef]
10. Gao, F.; Zhao, D.-L.; Li, Y.; Li, X.-G. Preparation and Hydrogen Storage of Activated Rayon-Based Carbon Fibers with High Specific Surface Area. *J. Phys. Chem. Solids* **2010**, *71*, 444–447. [CrossRef]
11. Moussa, M.; Bader, N.; Querejeta, N.; Durán, I.; Pevida, C.; Ouederni, A. Toward Sustainable Hydrogen Storage and Carbon Dioxide Capture in Post-Combustion Conditions. *J. Environ. Chem. Eng.* **2017**, *5*, 1628–1637. [CrossRef]
12. Sethia, G.; Sayari, A. Activated Carbon with Optimum Pore Size Distribution for Hydrogen Storage. *Carbon N. Y.* **2016**, *99*, 289–294. [CrossRef]
13. Doğan, M.; Sabaz, P.; Bïcïl, Z.; Koçer Kizilduman, B.; Turhan, Y. Activated Carbon Synthesis from Tangerine Peel and Its Use in Hydrogen Storage. *J. Energy Inst.* **2020**, *93*, 2176–2185. [CrossRef]
14. Rahimi, M.; Abbaspour-Fard, M.H.; Rohani, A.; Yuksel Orhan, O.; Li, X. Modeling and Optimizing N/O-Enriched Bio-Derived Adsorbents for CO2 Capture: Machine Learning and DFT Calculation Approaches. *Ind. Eng. Chem. Res.* **2022**, *61*, 10670–10688. [CrossRef]
15. Attia, N.F.; Jung, M.; Park, J.; Jang, H.; Lee, K.; Oh, H. Flexible Nanoporous Activated Carbon Cloth for Achieving High H2, CH4, and CO2 Storage Capacities and Selective CO2/CH4 Separation. *Chem. Eng. J.* **2020**, *379*, 122367. [CrossRef]
16. Attia, N.F.; Jung, M.; Park, J.; Cho, S.-Y.; Oh, H. Facile Synthesis of Hybrid Porous Composites and Its Porous Carbon for Enhanced H2 and CH4 Storage. *Int. J. Hydrogen Energy* **2020**, *45*, 32797–32807. [CrossRef]
17. Paraskevopoulou, V.; Artiaga, V.G.; Rowlinson, R.; Winkler, G.S.; Gellert, P.; Stolnik, S.; Overman, R.; Falcone, F.H. Introduction of a C-Terminal Hexa-Lysine Tag Increases Thermal Stability of the LacDiNac Binding Adhesin (LabA) Exodomain from Helicobacter Pylori. *Protein Expr. Purif.* **2019**, *163*, 105446. [CrossRef] [PubMed]
18. Schaefer, S.; Jeder, A.; Sdanghi, G.; Gadonneix, P.; Abdedayem, A.; Izquierdo, M.T.; Maranzana, G.; Ouederni, A.; Celzard, A.; Fierro, V. Oxygen-Promoted Hydrogen Adsorption on Activated and Hybrid Carbon Materials. *Int. J. Hydrogen Energy* **2020**, *45*, 30767–30782. [CrossRef]
19. Hu, W.; Huang, J.; Yu, P.; Zheng, M.; Xiao, Y.; Dong, H.; Liang, Y.; Hu, H.; Liu, Y. Hierarchically Porous Carbon Derived from Neolamarckia Cadamba for Electrochemical Capacitance and Hydrogen Storage. *ACS Sustain. Chem. Eng.* **2019**, *7*, 15385–15393. [CrossRef]
20. Üner, O.; Geçgel, Ü.; Avcu, T. Comparisons of Activated Carbons Produced from Sycamore Balls, Ripe Black Locust Seed Pods, and Nerium Oleander Fruits and Also Their H2 Storage Studies. *Carbon Lett.* **2020**, *31*, 75–92. [CrossRef]

21. Zhao, W.; Fierro, V.; Zlotea, C.; Aylon, E.; Izquierdo, M.T.; Latroche, M.; Celzard, A. Activated Carbons with Appropriate Micropore Size Distribution for Hydrogen Adsorption. *Int. J. Hydrogen Energy* **2011**, *36*, 5431–5434. [CrossRef]
22. Blankenship, L.S.; Mokaya, R. Cigarette Butt-Derived Carbons Have Ultra-High Surface Area and Unprecedented Hydrogen Storage Capacity. *Energy Environ. Sci.* **2017**, *10*, 2552–2562. [CrossRef]
23. Llorens, J.; Pera-Titus, M. Influence of Surface Heterogeneity on Hydrogen Adsorption on Activated Carbons. *Colloids Surfaces A Physicochem. Eng. Asp.* **2009**, *350*, 63–72. [CrossRef]
24. Yu, H.; Luo, H.; Cai, J.; Dong, C. Molecular and Atomic Adsorptions of Hydrogen, Oxygen, and Nitrogen on Defective Carbon Nanotubes: A First-Principles Study. *Int. J. Hydrogen Energy* **2020**, *45*, 26655–26665. [CrossRef]
25. Li, Y.; Liu, H. Grand Canonical Monte Carlo Simulation on the Hydrogen Storage Behaviors of the Cup-Stacked Carbon Nanotubes at Room Temperature. *Int. J. Hydrogen Energy* **2021**, *46*, 6623–6631. [CrossRef]
26. Parsaeian, M.; Rahimi, M.; Rohani, A.; Lawson, S.S. Towards the Modeling and Prediction of the Yield of Oilseed Crops: A Multi-Machine Learning Approach. *Agriculture* **2022**, *12*, 1739. [CrossRef]
27. Rahimi, M.; Pourramezan, M.-R.; Rohani, A. Modeling and Classifying the In-Operando Effects of Wear and Metal Contaminations of Lubricating Oil on Diesel Engine: A Machine Learning Approach. *Expert Syst. Appl.* **2022**, *203*, 117494. [CrossRef]
28. Butler, K.T.; Davies, D.W.; Cartwright, H.; Isayev, O.; Walsh, A. Machine Learning for Molecular and Materials Science. *Nature* **2018**, *559*, 547–555. [CrossRef]
29. Mashhadimoslem, H.; Vafaeinia, M.; Safarzadeh, M.; Ghaemi, A.; Fathalian, F.; Maleki, A. Development of Predictive Models for Activated Carbon Synthesis from Different Biomass for CO2 Adsorption Using Artificial Neural Networks. *Ind. Eng. Chem. Res.* **2021**, *60*, 13950–13966. [CrossRef]
30. Vakili, A.R.; Ehtesham, S.; Danesh-Mesgaran, M.; Rohani, A.; Rahimi, M. Toward Modeling the In Vitro Gas Production Process by Using Propolis Extract Oil Treatment: Machine Learning and Kinetic Models. *Ind. Eng. Chem. Res.* **2022**. [CrossRef]
31. Mashhadimoslem, H.; Ghaemi, A. Machine Learning Analysis and Prediction of N2, N2O, and O2 Adsorption on Activated Carbon and Carbon Molecular Sieve. *Environ. Sci. Pollut. Res.* **2022**, *30*, 4166–4186. [CrossRef]
32. Kolbadinejad, S.; Mashhadimoslem, H.; Ghaemi, A.; Bastos-Neto, M. Deep Learning Analysis of Ar, Xe, Kr, and O2 Adsorption on Activated Carbon and Zeolites Using ANN Approach. *Chem. Eng. Process.-Process Intensif.* **2022**, *170*, 108662. [CrossRef]
33. Rahimi, M.; Abbaspour-Fard, M.H.; Rohani, A. Machine Learning Approaches to Rediscovery and Optimization of Hydrogen Storage on Porous Bio-Derived Carbon. *J. Clean. Prod.* **2021**, *329*, 129714. [CrossRef]
34. Xiao, J.; Bi, C.; Pierre, B. ScienceDirect Neural Network Based Optimization for Cascade Filling Process of On-Board Hydrogen Tank. *Int. J. Hydrogen Energy* **2020**, *46*, 2936–2951. [CrossRef]
35. Yildiz, Z.; Uzun, H. Prediction of gas storage capacities in metal organic frameworks using artificial neural network. *Microporous Mesoporous Mater.* **2015**, *208*, 50–54. [CrossRef]
36. Kumar, K.V.; Castro, M.M. De Neural Network and Principal Component Analysis for Modeling of Hydrogen Adsorption Isotherms on KOH Activated Pitch-Based Carbons Containing Different Heteroatoms. *Chem. Eng. J.* **2010**, *159*, 272–279. [CrossRef]
37. Sun, Y.; DeJaco, R.F.; Li, Z.; Tang, D.; Glante, S.; Sholl, D.S.; Colina, C.M.; Snurr, R.Q.; Thommes, M.; Hartmann, M. Fingerprinting Diverse Nanoporous Materials for Optimal Hydrogen Storage Conditions Using Meta-Learning. *Sci. Adv.* **2021**, *7*, eabg3983. [CrossRef] [PubMed]
38. Anderson, G.; Schweitzer, B.; Anderson, R.; Gómez-Gualdrón, D.A. Attainable Volumetric Targets for Adsorption-Based Hydrogen Storage in Porous Crystals: Molecular Simulation and Machine Learning. *J. Phys. Chem. C* **2018**, *123*, 120–130. [CrossRef]
39. Thornton, A.W.; Simon, C.M.; Kim, J.; Kwon, O.; Deeg, K.S.; Konstas, K.; Pas, S.J.; Hill, M.R.; Winkler, D.A.; Haranczyk, M. Materials Genome in Action: Identifying the Performance Limits of Physical Hydrogen Storage. *Chem. Mater.* **2017**, *29*, 2844–2854. [CrossRef]
40. Sun, Y.; Xue, J.; Dong, S.; Zhang, Y.; An, Y.; Ding, B.; Zhang, T.; Dou, H.; Zhang, X. Biomass-Derived Porous Carbon Electrodes for High-Performance Supercapacitors. *J. Mater. Sci.* **2020**, *55*, 5166–5176. [CrossRef]
41. Breiman, L.E.O. Random Forests. *Mach. Learn.* **2001**, *45*, 5–32. [CrossRef]
42. Zhou, Z.; Wang, Y.; Li, M. Feature Selection Method Based on Hybrid SA-GA and Random Forests. In Proceedings of the 2020 International Conference on Computing and Data Science, CDS 2020, Stanford, CA, USA, 1–2 August 2020; pp. 139–142.
43. Safaei-Farouji, M.; Vo Thanh, H.; Dai, Z.; Mehbodniya, A.; Rahimi, M.; Ashraf, U.; Radwan, A.E. Exploring the Power of Machine Learning to Predict Carbon Dioxide Trapping Efficiency in Saline Aquifers for Carbon Geological Storage Project. *J. Clean. Prod.* **2022**, *372*, 133778. [CrossRef]
44. Breiman, L. *Classification and Regression Trees*; Routledge: London, UK, 2017; ISBN 0412048418.
45. Chen, B.; Pawar, R.J. Characterization of CO2 Storage and Enhanced Oil Recovery in Residual Oil Zones. *Energy* **2019**, *183*, 291–304. [CrossRef]
46. Pedregosa, F.; Weiss, R.; Brucher, M. Scikit-Learn: Machine Learning in Python. *J. Mach. Learn. Res.* **2011**, *12*, 2825–2830.
47. Kennedy, J.; Eberhart, R. Particle Swarm Optimization. In Proceedings of the ICNN'95—International Conference on Neural Networks, Perth, Australia, 27 November–1 December 1995; pp. 1942–1948.
48. Del Valle, Y.; Venayagamoorthy, G.K.; Mohagheghi, S.; Hernandez, J.C.; Harley, R.G. Particle Swarm Optimization: Basic Concepts, Variants and Applications in Power Systems. *IEEE Trans. Evol. Comput.* **2008**, *12*, 171–195. [CrossRef]

49. Herrera, F.; Lozano, M.; Verdegay, J.L. Tackling Real-Coded Genetic Algorithms: Operators and Tools for Behavioural Analysis. *Artif. Intell. Rev.* **1998**, *12*, 265–319. [CrossRef]
50. Rahimi, M.; Abbaspour-Fard, M.H.; Rohani, A. Synergetic Effect of N/O Functional Groups and Microstructures of Activated Carbon on Supercapacitor Performance by Machine Learning. *J. Power Sources* **2022**, *521*, 230968. [CrossRef]
51. Le, L.T.; Nguyen, H.; Dou, J.; Zhou, J. A Comparative Study of PSO-ANN, GA-ANN, ICA-ANN, and ABC-ANN in Estimating the Heating Load of Buildings ' Energy E Ffi Ciency for Smart City Planning. *Appl. Sci.* **2019**, *9*, 2630. [CrossRef]
52. Zheng, Y.; Huang, M.; Lu, Y.; Li, W. Fractional Stochastic Resonance Multi-Parameter Adaptive Optimization Algorithm Based on Genetic Algorithm. *Neural Comput. Appl.* **2020**, *32*, 16807–16818. [CrossRef]
53. Ali, M.; Jiang, R.; Huolin, M.; Pan, H.; Abbas, K.; Ashraf, U.; Ullah, J. Machine Learning-A Novel Approach of Well Logs Similarity Based on Synchronization Measures to Predict Shear Sonic Logs. *J. Pet. Sci. Eng.* **2021**, *203*, 108602. [CrossRef]
54. Mirjalili, S.; Mirjalili, S.M.; Lewis, A. Grey Wolf Optimizer. *Adv. Eng. Softw.* **2014**, *69*, 46–61. [CrossRef]
55. Hammouri, A.I.; Mafarja, M.; Al-Betar, M.A.; Awadallah, M.A.; Abu-Doush, I. An Improved Dragonfly Algorithm for Feature Selection. *Knowledge-Based Syst.* **2020**, *203*, 106131. [CrossRef]
56. Mirjalili, S. Dragonfly Algorithm: A New Meta-Heuristic Optimization Technique for Solving Single-Objective, Discrete, and Multi-Objective Problems. *Neural Comput. Appl.* **2016**, *27*, 1053–1073. [CrossRef]
57. Reynolds, C.W. Flocks, Herds, and Schools: A Distributed Behavioral Model. *Comput. Graph.* **1987**, *21*, 25–34. [CrossRef]
58. Bader, N.; Ouederni, A. Functionalized and Metal-Doped Biomass-Derived Activated Carbons for Energy Storage Application. *J. Energy Storage* **2017**, *13*, 268–276. [CrossRef]
59. Balahmar, N.; Mokaya, R. Pre-Mixed Precursors for Modulating the Porosity of Carbons for Enhanced Hydrogen Storage: Towards Predicting the Activation Behaviour of Carbonaceous Matter. *J. Mater. Chem. A* **2019**, *7*, 17466–17479. [CrossRef]
60. Zhao, W.; Luo, L.; Chen, T.; Li, Z.; Zhang, Z.; Wang, H.; Rao, J.; Feo, L.; Fan, M. Synthesis and Characterization of Pt-N-Doped Activated Biocarbon Composites for Hydrogen Storage. *Compos. Part B Eng.* **2019**, *161*, 464–472. [CrossRef]
61. Rossetti, I.; Ramis, G.; Gallo, A.; Di Michele, A. Hydrogen Storage over Metal-Doped Activated Carbon. *Int. J. Hydrogen Energy* **2015**, *40*, 7609–7616. [CrossRef]
62. Pedicini, R.; Maisano, S.; Chiodo, V.; Conte, G.; Policicchio, A.; Agostino, R.G. Posidonia Oceanica and Wood Chips Activated Carbon as Interesting Materials for Hydrogen Storage. *Int. J. Hydrogen Energy* **2020**, *45*, 14038–14047. [CrossRef]
63. Bader, N.; Ouederni, A. Optimization of Biomass-Based Carbon Materials for Hydrogen Storage. *J. Energy Storage* **2016**, *5*, 77–84. [CrossRef]
64. Sangchoom, W.; Mokaya, R. Valorization of Lignin Waste: Carbons from Hydrothermal Carbonization of Renewable Lignin as Superior Sorbents for CO2 and Hydrogen Storage. *ACS Sustain. Chem. Eng.* **2015**, *3*, 1658–1667. [CrossRef]
65. Minoda, A.; Oshima, S.; Iki, H.; Akiba, E. Synthesis of KOH-Activated Porous Carbon Materials and Study of Hydrogen Adsorption. *J. Alloys Compd.* **2013**, *580*, S301–S304. [CrossRef]
66. González-Navarro, M.F.; Giraldo, L.; Moreno-Piraján, J.C. Preparation and Characterization of Activated Carbon for Hydrogen Storage from Waste African Oil-Palm by Microwave-Induced LiOH Basic Activation. *J. Anal. Appl. Pyrolysis* **2014**, *107*, 82–86. [CrossRef]
67. Fierro, V.; Zhao, W.; Izquierdo, M.T.; Aylon, E.; Celzard, A. Adsorption and Compression Contributions to Hydrogen Storage in Activated Anthracites. *Int. J. Hydrogen Energy* **2010**, *35*, 9038–9045. [CrossRef]
68. Jang, H.S.; Mun, J.; Hong, W.G.; Lee, S.M.; Jeon, J.W.; Lee, C.Y.; Kim, H.J.; Kim, B.H. The Performance of Green Carbon as a Backbone for Hydrogen Storage Materials. *Int. J. Hydrogen Energy* **2020**, *45*, 10516–10522. [CrossRef]
69. Stelitano, S.; Conte, G.; Policicchio, A.; Aloise, A.; Desiderio, G.; Agostino, R.G. Pinecone-Derived Activated Carbons as an Effective Medium for Hydrogen Storage. *Energies* **2020**, *13*, 2237. [CrossRef]
70. Park, J.H.; Park, S.J. Expansion of Effective Pore Size on Hydrogen Physisorption of Porous Carbons at Low Temperatures with High Pressures. *Carbon N. Y.* **2020**, *158*, 364–371. [CrossRef]
71. Figueroa-Torres, M.Z.; Domínguez-Ríos, C.; Cabañas-Moreno, J.G.; Vega-Becerra, O.; Aguilar-Elguézabal, A. The Synthesis of Ni-Activated Carbon Nanocomposites via Electroless Deposition without a Surface Pretreatment as Potential Hydrogen Storage Materials. *Int. J. Hydrogen Energy* **2012**, *37*, 10743–10749. [CrossRef]
72. Ramesh, T.; Rajalakshmi, N.; Dhathathreyan, K.S. Synthesis and Characterization of Activated Carbon from Jute Fibers for Hydrogen Storage. *Renew. Energy Environ. Sustain.* **2017**, *2*, 4. [CrossRef]
73. Lee, S.Y.; Park, S.J. Effect of Platinum Doping of Activated Carbon on Hydrogen Storage Behaviors of Metal-Organic Frameworks-5. *Int. J. Hydrogen Energy* **2011**, *36*, 8381–8387. [CrossRef]
74. Zhao, W.; Fierro, V.; Zlotea, C.; Aylon, E.; Izquierdo, M.T.; Latroche, M.; Celzard, A. Optimization of Activated Carbons for Hydrogen Storage. *Int. J. Hydrogen Energy* **2011**, *36*, 11746–11751. [CrossRef]
75. Xiao, Y.; Dong, H.; Long, C.; Zheng, M.; Lei, B.; Zhang, H.; Liu, Y. Melaleuca Bark Based Porous Carbons for Hydrogen Storage. *Int. J. Hydrogen Energy* **2014**, *39*, 11661–11667. [CrossRef]
76. Tellez-Juárez, M.C.; Fierro, V.; Zhao, W.; Fernández-Huerta, N.; Izquierdo, M.T.; Reguera, E.; Celzard, A. Hydrogen Storage in Activated Carbons Produced from Coals of Different Ranks: Effect of Oxygen Content. *Int. J. Hydrogen Energy* **2014**, *39*, 4996–5002. [CrossRef]
77. Akasaka, H.; Takahata, T.; Toda, I.; Ono, H.; Ohshio, S.; Himeno, S.; Kokubu, T.; Saitoh, H. Hydrogen Storage Ability of Porous Carbon Material Fabricated from Coffee Bean Wastes. *Int. J. Hydrogen Energy* **2011**, *36*, 580–585. [CrossRef]

78. Heo, Y.; Park, S. Journal of Industrial and Engineering Chemistry Synthesis of Activated Carbon Derived from Rice Husks for Improving Hydrogen Storage Capacity. *J. Ind. Eng. Chem.* **2015**, *31*, 330–334. [CrossRef]
79. Xia, K.; Hu, J.; Jiang, J. Enhanced Room-Temperature Hydrogen Storage in Super-Activated Carbons: The Role of Porosity Development by Activation. *Appl. Surf. Sci.* **2014**, *315*, 261–267. [CrossRef]
80. Zyzlila Figueroa-Torres, M.; Robau-Sánchez, A.; De la Torre-Sáenz, L.; Aguilar-Elguézabal, A. Hydrogen Adsorption by Nanostructured Carbons Synthesized by Chemical Activation. *Microporous Mesoporous Mater.* **2007**, *98*, 89–93. [CrossRef]
81. Ramesh, T.; Rajalakshmi, N.; Dhathathreyan, K.S. Activated Carbons Derived from Tamarind Seeds for Hydrogen Storage. *J. Energy Storage* **2015**, *4*, 89–95. [CrossRef]
82. Jiménez, V.; Sánchez, P.; Díaz, J.A.; Valverde, J.L.; Romero, A. Hydrogen Storage Capacity on Different Carbon Materials. *Chem. Phys. Lett.* **2010**, *485*, 152–155. [CrossRef]
83. Geng, Z.; Wang, D.; Zhang, C.; Zhou, X.; Xin, H.; Liu, X.; Cai, M. Spillover Enhanced Hydrogen Uptake of Pt/Pd Doped Corncob-Derived Activated Carbon with Ultra-High Surface Area at High Pressure. *Int. J. Hydrogen Energy* **2014**, *39*, 13643–13649. [CrossRef]
84. Zhang, C.; Geng, Z.; Cai, M.; Zhang, J.; Liu, X.; Xin, H.; Ma, J. Microstructure Regulation of Super Activated Carbon from Biomass Source Corncob with Enhanced Hydrogen Uptake. *Int. J. Hydrogen Energy* **2013**, *38*, 9243–9250. [CrossRef]
85. Balathanigaimani, M.S.; Haider, B.; Jha, D.; Kumar, R.; Lee, S.J.; Shim, W.G.; Shon, H.K.; Kim, S.C.; Moon, H. Nanostructured Biomass Based Carbon Materials from Beer Lees for Hydrogen Storage. *J. Nanosci. Nanotechnol.* **2018**, *18*, 2196–2199. [CrossRef] [PubMed]
86. Li, X.; Zhang, H.; Zhao, B.; Zhang, Y. Preparation of Hydrogen Storage Carbon Materials Using Bio-Oil Heavy Components as Carbon-Containing Precursor. *Fuel Process. Technol.* **2020**, *203*, 106386. [CrossRef]
87. Fierro, V.; Szczurek, A.; Zlotea, C.; Marêché, J.F.; Izquierdo, M.T.; Albiniak, A.; Latroche, M.; Furdin, G.; Celzard, A. Experimental Evidence of an Upper Limit for Hydrogen Storage at 77 K on Activated Carbons. *Carbon N. Y.* **2010**, *48*, 1902–1911. [CrossRef]
88. Chen, H.; Wang, H.; Xue, Z.; Yang, L.; Xiao, Y.; Zheng, M.; Lei, B.; Liu, Y.; Sun, L. High Hydrogen Storage Capacity of Rice Hull Based Porous Carbon. *Int. J. Hydrogen Energy* **2012**, *37*, 18888–18894. [CrossRef]
89. Jordá-Beneyto, M.; Suárez-García, F.; Lozano-Castelló, D.; Cazorla-Amorós, D.; Linares-Solano, A. Hydrogen Storage on Chemically Activated Carbons and Carbon Nanomaterials at High Pressures. *Carbon N. Y.* **2007**, *45*, 293–303. [CrossRef]
90. Choi, Y.K.; Park, S.J. Hydrogen Storage Capacity of Highly Porous Carbons Synthesized from Biomass-Derived Aerogels. *Carbon Lett.* **2015**, *16*, 127–131. [CrossRef]
91. Sun, Y.; Webley, P.A. Preparation of Activated Carbons from Corncob with Large Specific Surface Area by a Variety of Chemical Activators and Their Application in Gas Storage. *Chem. Eng. J.* **2010**, *162*, 883–892. [CrossRef]
92. Wang, J.; Senkovska, I.; Kaskel, S.; Liu, Q. Chemically Activated Fungi-Based Porous Carbons for Hydrogen Storage. *Carbon N. Y.* **2014**, *75*, 372–380. [CrossRef]
93. Chen, T.; Zhou, Y.; Luo, L.; Wu, X.; Li, Z.; Fan, M.; Zhao, W. Preparation and Characterization of Heteroatom Self-Doped Activated Biocarbons as Hydrogen Storage and Supercapacitor Electrode Materials. *Electrochim. Acta* **2019**, *325*. [CrossRef]
94. Huang, C.C.; Chen, H.M.; Chen, C.H.; Huang, J.C. Effect of Surface Oxides on Hydrogen Storage of Activated Carbon. *Sep. Purif. Technol.* **2010**, *70*, 291–295. [CrossRef]
95. Kopac, T.; Kırca, Y. Effect of Ammonia and Boron Modifications on the Surface and Hydrogen Sorption Characteristics of Activated Carbons from Coal. *Int. J. Hydrogen Energy* **2020**, *45*, 10494–10506. [CrossRef]
96. Wang, H.; Gao, Q.; Hu, J. High Hydrogen Storage Capacity of Porous Carbons Prepared by Using Activated Carbon. *J. Am. Chem. Soc.* **2009**, *131*, 7016–7022. [CrossRef]
97. Hwang, S.H.; Choi, W.M.; Lim, S.K. Hydrogen Storage Characteristics of Carbon Fibers Derived from Rice Straw and Paper Mulberry. *Mater. Lett.* **2016**, *167*, 18–21. [CrossRef]
98. Jin, H.; Lee, Y.S.; Hong, I. Hydrogen Adsorption Characteristics of Activated Carbon. *Catal. Today* **2007**, *120*, 399–406. [CrossRef]
99. Parthasarathy, P.; Narayanan, S.K. Effect of Hydrothermal Carbonization Reaction Parameters On. *Environ. Prog. Sustain. Energy* **2014**, *33*, 676–680. [CrossRef]
100. Yang, R.; Liu, G.; Li, M.; Zhang, J.; Hao, X. Preparation and N 2, CO 2 and H 2 Adsorption of Super Activated Carbon Derived from Biomass Source Hemp (*Cannabis Sativa* L.) Stem. *Microporous Mesoporous Mater.* **2012**, *158*, 108–116. [CrossRef]
101. Melouki, R.; Llewellyn, P.L.; Tazibet, S.; Boucheffa, Y. Hydrogen Adsorption on Activated Carbons Prepared from Olive Waste: Effect of Activation Conditions on Uptakes and Adsorption Energies. *J. Porous Mater.* **2017**, *24*. [CrossRef]
102. Liu, X.; Zhang, C.; Geng, Z.; Cai, M. High-Pressure Hydrogen Storage and Optimizing Fabrication of Corncob-Derived Activated Carbon. *Microporous Mesoporous Mater.* **2014**, *194*, 60–65. [CrossRef]
103. Rowlandson, J.L.; Edler, K.J.; Tian, M.; Ting, V.P. Toward Process-Resilient Lignin-Derived Activated Carbons for Hydrogen Storage Applications. *ACS Sustain. Chem. Eng.* **2020**, *8*, 2186–2195. [CrossRef]
104. Wang, D.; Geng, Z.; Zhang, C.; Zhou, X.; Liu, X. Effects of Thermal Activation Conditions on the Microstructure Regulation of Corncob-Derived Activated Carbon for Hydrogen Storage. *J. Energy Chem.* **2014**, *23*, 601–608. [CrossRef]
105. Wróbel-Iwaniec, I.; Díez, N.; Gryglewicz, G. Chitosan-Based Highly Activated Carbons for Hydrogen Storage. *Int. J. Hydrogen Energy* **2015**, *40*, 5788–5796. [CrossRef]
106. Zieliński, M.; Wojcieszak, R.; Monteverdi, S.; Mercy, M.; Bettahar, M.M. Hydrogen Storage on Nickel Catalysts Supported on Amorphous Activated Carbon. *Catal. Commun.* **2005**, *6*, 777–783. [CrossRef]

107. Sevilla, M.; Fuertes, A.B.; Mokaya, R. High Density Hydrogen Storage in Superactivated Carbons from Hydrothermally Carbonized Renewable Organic Materials. *Energy Environ. Sci.* **2011**, *4*, 1400–1410. [CrossRef]
108. Cheng, F.; Liang, J.; Zhao, J.; Tao, Z.; Chen, J. Biomass Waste-Derived Microporous Carbons with Controlled Texture and Enhanced Hydrogen Uptake. *Chem. Mater.* **2008**, *20*, 1889–1895. [CrossRef]
109. Md Arshad, S.H.; Ngadi, N.; Aziz, A.A.; Amin, N.S.; Jusoh, M.; Wong, S. Preparation of Activated Carbon from Empty Fruit Bunch for Hydrogen Storage. *J. Energy Storage* **2016**, *8*, 257–261. [CrossRef]